Oxygen Degradation in Mesoporous $Al_2O_3/CH_3NH_3PbI_{3-x}Cl_x$ Perovskite Solar Cells: Kinetics and Mechanisms

Andrew J. Pearson, Giles E. Eperon, Paul E. Hopkinson, Severin N. Habisreutinger, Jacob Tse-Wei Wang, Henry J. Snaith, and Neil C. Greenham**

The rapid pace of development for hybrid perovskite photovoltaics has recently resulted in promising figures of merit being obtained with regard to device stability. Rather than relying upon expensive barrier materials, realizing market-competitive lifetimes is likely to require the development of intrinsically stable devices, and to this end accelerated aging tests can help identify degradation mechanisms that arise over the long term. Here, oxygen-induced degradation of archetypal perovskite solar cells under operation is observed, even in dry conditions. With prolonged aging, this process ultimately drives decomposition of the perovskite. It is deduced that this is related to charge build-up in the perovskite layer, and it is shown that by efficiently extracting charge this degradation can be mitigated. The results confirm the importance of high charge-extraction efficiency in maximizing the tolerance of perovskite solar cells to oxygen.

1. Introduction

Solution-processed organic–inorganic (hybrid) halide perovskites have emerged as a promising family of semiconducting materials for photovoltaic (PV) applications.[1–5] The unexpectedly clean electronic properties of these semiconductors have led to the demonstration of proof-of-concept PV devices with an initial efficiency that outperforms competing 'next-generation' technologies such as dye-sensitized, organic, and quantum dot solar cells, and even matches that of commercially deployed PV.[6] Other attractive characteristics of hybrid perovskites include the low embedded costs of materials processing and the ability to tune the properties of the semiconductor through changes in chemical composition.[1,7–10] All of these factors have led to hybrid perovskites being considered as disruptive materials in a wide range of technology applications;[11–16] interest from the materials science research community is both substantial and rapidly maturing.

Realizing the technology potential of hybrid perovskites necessitates a thorough understanding of the degradation mechanisms that limit the lifetime of devices, and identifying solutions to mitigate these. This exercise is nontrivial because of the various factors that can affect device performance: light, heat, moisture, oxygen, mechanical and electrical stresses, and combinations thereof.[17,18] Currently, perovskite solar cells (PSCs) based on the "triple layer" architecture with a thick carbon back electrode have demonstrated perhaps the most stable performance characteristics of all PSCs.[19] These devices, based on the mixed cation perovskite $(5\text{-AVA})_x(MA)_{1-x}PbI_3$ (where 5-AVA corresponds to 5-ammoniumvaleric acid), have been shown to maintain their initial power conversion efficiency (PCE) of approximately 10% over 1000 h continuous simulated solar illumination,[20] dark storage for three months at elevated temperatures and humidity (85 °C/85%) and a minimum of 7 d operation in real-world conditions (Jeddah, Saudi Arabia).[21] Although clearly commendable, it is apparent that significant work is required to realize PSCs with high stability and high performance, where promising stability metrics are combined with the certified PCE values for champion devices.[22]

To elucidate the underlying mechanisms for degradation in hybrid perovskites and guide the development of intrinsically stable devices, considerable work has been undertaken on the archetypal semiconductor of the research field: $CH_3NH_3PbI_3$. It is known that this material (and other single or mixed-halide derivatives) are particularly sensitive to moisture,[1,7,17,23–26] where the proposed chemical reactions involving water result in decomposition of the perovskite into its precursor components via

Dr. A. J. Pearson, Prof. N. C. Greenham
Cavendish Laboratory
J. J. Thomson Avenue, Cambridge CB3 0HE, UK
E-mail: ncg11@cam.ac.uk
Dr. G. E. Eperon,[+] S. N. Habisreutinger, J. T.-W. Wang, Prof. H. J. Snaith
Clarendon Laboratory
University of Oxford
Parks Road, Oxford OX1 3PU, UK
E-mail: henry.snaith@physics.ox.ac.uk
Dr. P. E. Hopkinson
Centre for Advanced Materials
Universität Heidelberg
Heidelberg 69120, Germany
Dr. P. E. Hopkinson
Kirchhoff-Institut für Physik
Universität Heidelberg
Heidelberg 69120, Germany
[+]Present Address: Department of Chemistry, University of Washington Seattle, Washington 98195, United States.

DOI: 10.1002/aenm.201600014

intermediate and semi-reversible monohydrate phases.[17,26] The rate of decomposition is dependent on the preparation method of the perovskite sample and is accelerated by oxygen and heat.[27–29] However, the presence of some moisture during device processing has been shown to be somewhat beneficial for material quality and solar cell performance, owing to a reduced trap density in films. However, the stability of devices prepared in the presence of moisture is still an open question owing to the absence of promising lifetime data.[30,31] Hybrid perovskite films containing aprotic organic cations have been suggested[32] and shown[33] to exhibit improved intrinsic moisture tolerance, the latter inferred through powder X-ray diffraction (XRD) studies. Nevertheless, the moisture stability of $CH_3NH_3PbI_3$ can be improved at the device level by employing various engineering strategies during fabrication of the PSC. Substitution of the doped spiro-MeOTAD hole transport layer for undoped tetrathiafulvalene derivatives[34] or carbon nanotubes embedded in a polymer matrix[27] have been demonstrated as effective modifications for imparting greater moisture tolerance, the latter also improving thermal stability.

In dry conditions, understanding the effects of oxygen on PSCs is perhaps less well understood. Device stability work in this specific area has so far been limited to dark storage tests[2,35] which provide no insight into the prolonged interplay between light, oxygen, and biasing on a working PSC. To address this issue, we characterize the behavior of a model PSC in the presence of oxygen, improving our understanding of the factors affecting the stability of this promising technology. Alongside standard IV measurements, transient photocurrent/photovoltage (TPC/TPV) measurements were conducted in situ, i.e., in sequence with the IV scans, to gain partial access to the dynamics of photocurrent generation during accelerated aging. Combined with optical microscopy and XRD measurements, a relatively detailed insight into the evolution of the solar cells during our controlled aging tests is obtained. These complementary experiments provide sufficient information to identify the underlying causes of degradation in our model system and provide a framework for engineering PSCs with enhanced oxygen tolerance, an important contribution to the realization of PSCs with market-competitive lifetimes.

2. Results and Discussion

In **Figure 1**, we show the initial photovoltaic characteristics of $CH_3NH_3PbI_{3-X}Cl_X$ PSCs employing a mesoporous alumina scaffold (the reference solar cells)[2,36] and lifetime data during aging in the presence of O_2. Compact TiO_2 and doped Spiro-MeOTAD were used as electron- and hole-transporting layers, respectively, in the reference solar cells (see the Experimental Section for details). For each device, an initial stabilized PCE was determined by first measuring the cell photocurrent during a reverse bias scan and subsequently monitoring the photocurrent at the maximum

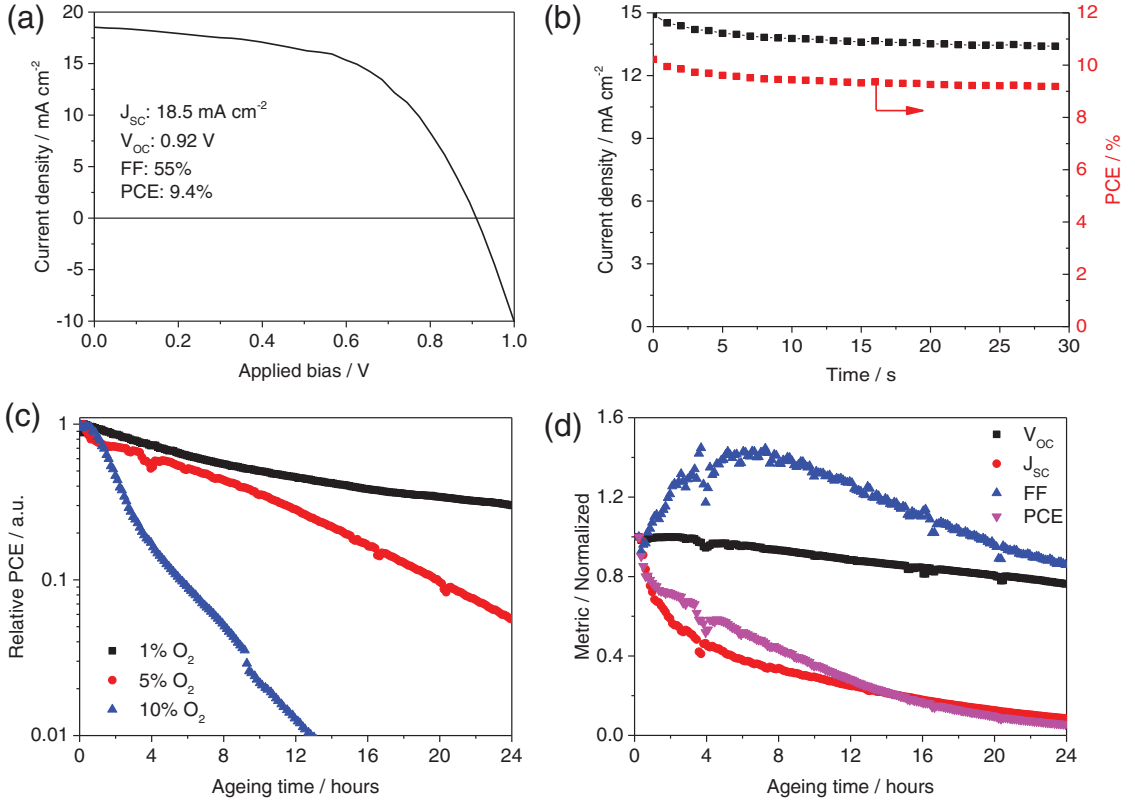

Figure 1. Solar cell characteristics for the device architecture studied in this work. a) Current–voltage curve of a typical device, as measured via reverse bias scan. b) Photocurrent and power conversion efficiency of the same device over 30 s continuous illumination at maximum power point, used to determine an initial quasi-stabilized PCE. c) Relative changes in solar cell power conversion efficiency (PCE) for different vol% of O_2 in the testing chamber atmosphere. Here, devices were first stabilized for 24 h under light and N_2 before stress testing. Each quantity is normalized to the efficiency of the solar cell after the stabilizing step. d) Relative changes in the photovoltaic metrics of a reference solar cell operating in an atmosphere of 5 vol% O_2.

power point until stable (Figure 1b). According to this protocol, the tested solar cells exhibited an initial PCE of 9 ± 1% across two device batch fabrications (see Figure 1a for typical metrics), with a champion efficiency of 11.1%. The distribution of solar cell PCEs is shown in the Supporting Information, Figure S1.

The stability of the reference solar cells under simulated AM 1.5 G solar illumination was monitored in a custom-built atmospheric chamber. Because our study is focused on the effects of oxygen, devices were first measured for 24 h under N_2 to confirm that the remaining environmental conditions do not trigger kinetic processes (such as "burn-in") that overlap on a comparable timescale. Specifically, this "stabilizing" step provided time for the PSCs to undergo limited burn-in (either positive or negative) due to continuous illumination, voltage biasing, and equilibrating to the chamber temperature (40–45 °C). Furthermore, a slow voltage scan (0–1 V, 0.05 V step size, 10 s wait) was employed throughout each experiment to balance the monitoring of individual solar cell metrics with conditions likely to be experienced in real world applications (i.e., maximum-power-point tracking). Unless explicitly stated, solar cell efficiency metrics correspond to an average of values obtained from slow forward and reverse bias scans. Figure S2–S4 in the Supporting Information provide additional information on our testing procedure.

Figure 1c,d presents the evolution in PCE of perovskite solar cells exposed to oxygen, where data correspond to testing chamber atmospheres with a fixed vol% of O_2 relative to N_2. Both gases were dry as confirmed by an external gas sensor. Throughout all aging tests, the atmospheric concentration of H_2O was typically 10–30 ppm, which should be insignificant for degradation over the timescales of the experiment. From Figure 1c, it can be seen that the PCE of the reference cells undergoes a dramatic reduction due to operating in an N_2/O_2 atmosphere. The severity of this process is clearly linked to the absolute vol% of O_2; after 24 h stress testing, 70% of the initial efficiency is lost when O_2 is present at 1 vol%. When the O_2 concentration is increased to 10 vol%, the same relative performance drop occurs after 2.7 h. Figure 1d gives further insight into the origin of the performance decrease, where data for the intermediate stress testing case of 5 vol% O_2 are presented. As shown, power conversion efficiency is primarily lost via a reduction in photocurrent density (J_{SC}). Losses in open circuit voltage (V_{OC}) are also observed, however the device fill factor undergoes a temporary increase during the early stages of stress testing before reducing, this behavior potentially reflecting changes in ionic mobility in the sample on a timescale that is commensurate with our slow voltage scans.[37]

We recognize that the perceived kinetics of degradation in PSCs may be influenced by measurement history alongside the conditions of the aging environment. PSCs routinely exhibit unstable current–voltage characteristics, described as either a "hysteresis effect"[38] or a "temporary current enhancement by bias".[39] The underlying origins for this behavior are still under debate,[38,40–42] however it is thought to involve the motion of ions or defects within the perovskite and their ability to adjust the built-in field of a solar cell during illumination or prebiasing, alongside the presence of electronic traps which facilitate trap-assisted recombination.[2,43–47] The timescales and temperatures over which hysteresis effects are observable depend strongly on the architecture of the PSC.[37,48–50] To appreciate how hysteresis may evolve during accelerated aging, one device was subject to sequential fast and slow bias scans in both a forward and reverse direction. As shown in the Supporting Information, Figure S5, once the solar cell is stabilized under N_2 the slow scans converge to give a reproducible PCE value. Fast bias scans result in an apparent enhancement (reverse direction) or reduction (forward direction) in PCE relative to the slow bias scans, in qualitative agreement with previous reports.[38] During accelerated aging under N_2/O_2, solar cell PCE undergoes a reduction regardless of the scan conditions used, however the slow scans eventually give a higher apparent PCE than the fast scans irrespective of the scan direction used. Work is ongoing to rationalize this behavior, however we hypothesize that it reflects a progressive increase of the forward bias stabilization time required to reach peak voltage and current, as compared to the time spent at forward bias in the fast scan routine. It has been empirically observed that cells which exhibit the most severe hysteresis generally require longer to reach stabilized photocurrent.[51] The increased timescale may be due to a combination of increased density of traps and mobile ionic species, in addition to a change in the activation energies underlying migration of ionic species.

To gain additional information about the effects of O_2 exposure, we consider the evolution in solar cell characteristics as measured through TPC and TPV. Individual measurements were averaged over ≈10 s, a period that is commensurate with the wait time used in our standard IV measurements. Results from TPC are shown in **Figure 2**.

In Figure 2a, the TPC current for the stabilized device is characterized by a prompt rise to a constant value when the LED is switched on. After the LED is switched off, the current undergoes a rapid fall with a small tail extending for a few tens of microseconds. This type of response is qualitatively indicative of a solar cell with good charge transport and extraction characteristics.[52–54] With increasing exposure time of the cell to O_2, we see the emergence of a decay in photocurrent at the end of the LED pulse. Following LED switch off, here highlighted in Figure 2b, the transient current becomes negative with increased aging of the solar cell (i.e., charge is being injected into the solar cell rather than being extracted). We clarify the kinetics of these processes in Figure 2c,d. Figure 2c shows a comparison between current values extracted immediately after the LED is switched on and just before it is switched off. Figure 2d shows the total extracted charge during the decay after the LED is switched off. From these figures it can be seen that the photocurrent immediately after LED switch on does not change until about 12 h into the stress test. Note that by this time the quasi-stabilized photocurrent has already undergone a substantial reduction: 64% as measured through TPC (photocurrent reading at the end of the LED pulse) and 80% as measured through IV, with the mismatch potentially arising from variations in photocurrent dependency on light intensity. Beyond 12 h, further reductions in photocurrent are correlated with the extracted charge becoming less negative.

We interpret these measurements as an indication that the PSC has undergone two distinct phases of degradation over the course of the experiment. For low cumulative O_2 exposure (i.e., before ≈12 h in this case), photocurrent loss is due to the formation of charge barriers at the PSC electrode interface layers that act to screen the built-in field, thereby reducing the efficiency of charge extraction.[41] The simultaneous emergence of a negative

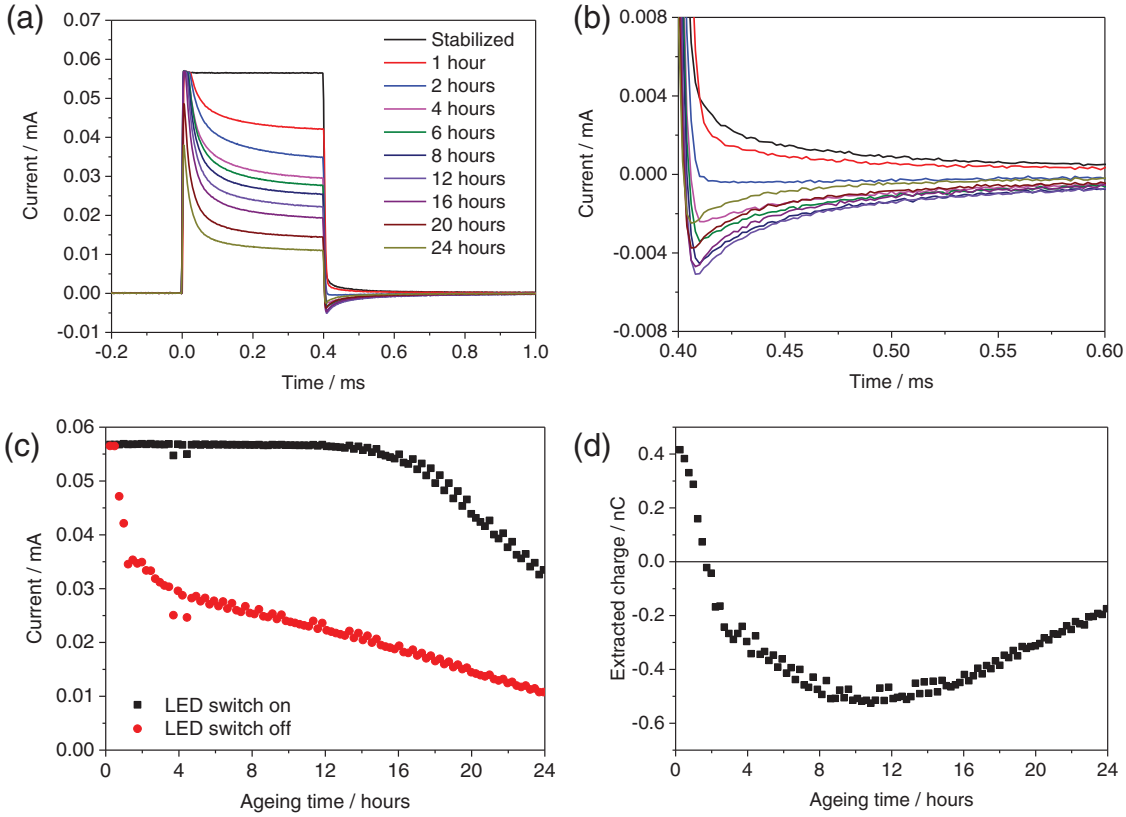

Figure 2. Transient photocurrent data for the reference solar cell aged under 5% O_2. a) TPC signal at distinct stages in the stress test, where 0 ms corresponds to the start of the 0.4 ms LED illumination pulse. b) A magnified region corresponding to the current decay ($t > 0.4$ ms, LED off). c) The evolution in TPC current throughout the aging test at two distinct points (LED switch on: averaged between 0.004 and 0.014 ms; LED switch off: quasi-stabilized photocurrent measured just before switch-off at 0.4 ms). d) The integrated current during the transient decay is plotted against aging time.

compensation current in the transient decay suggests that once the LED has been switched off, the solar cell retains an excess of trapped charge that continues to modify its internal electric field. In order for the device to be brought back to equilibrium, new charge must be injected into the cell to neutralize the trapped charge that is otherwise not extracted – a "compensation current", which will appears as negative here.[52] We propose that the underlying mechanism for the formation of charge barriers is an increase in the density of mobile defects (or ionic species) and electronic traps within the perovskite layer.[43,55] For the mobile defects, their activation energy is low enough to enable them to screen the built-in field on the timescale of hundreds of microseconds to seconds whilst the device is under illumination. This behavior is analogous to the way in which mobile defects are thought to affect JV scans, where holding at high voltages permits movement of defects in such a way as to enhance the field in the device and assist charge extraction (resulting in the enhanced reverse JV scan).[18,38] The compensation current is then related to the defects diffusing away from the electrodes and neutralization of the now built-up charge. These processes continue until, following extended O_2 exposure (after ≈12 h), a loss in transient photocurrent is eventually recorded at the beginning of the LED pulse. We use this relatively fast measurement as a proxy for photocurrent efficiency before poor extraction effects dominate the TPC dynamics. Because we observe lower instantaneous photocurrent in this second phase of the experiment, we propose that the perovskite itself has now undergone material degradation, more severe than just inducing defects. This damage will act to reduce the efficiency of light harvesting, and/or trigger sub-microsecond recombination of charge carriers that is otherwise not resolved during our TPC measurement. As a result of these specific losses, the magnitude of the compensation current required to neutralize the (now fewer) trapped charges after LED illumination decreases, as evidenced in Figure 2d.

To explore the idea of a two-stage degradation process, and determine the permanency of any efficiency loss in PSCs caused by operating with exposure to oxygen, we continued to monitor the device that had been aged under 1% O_2 (which underwent the smallest reduction in PCE after 24 h) after the oxygen supply to the sample chamber had been switched off. As shown in **Figure 3**, extended operation under dry nitrogen results in the partial recovery of PCE (≈30% of the initial value) that had otherwise been lost during operation with oxygen present. Data in Figure 3a show the close correlation between PCE evolution and changes in photocurrent, indicating that further insight can be provided by our in situ TPC measurements. TPC traces at distinct stages of this experiment are presented in Figure 3b, where it can be seen that recovery modifies the PSC photocurrent over hundreds of microseconds, this timescale being commensurate with the proposed screening process of the PSC built-in field discussed earlier. In addition, the recovery process

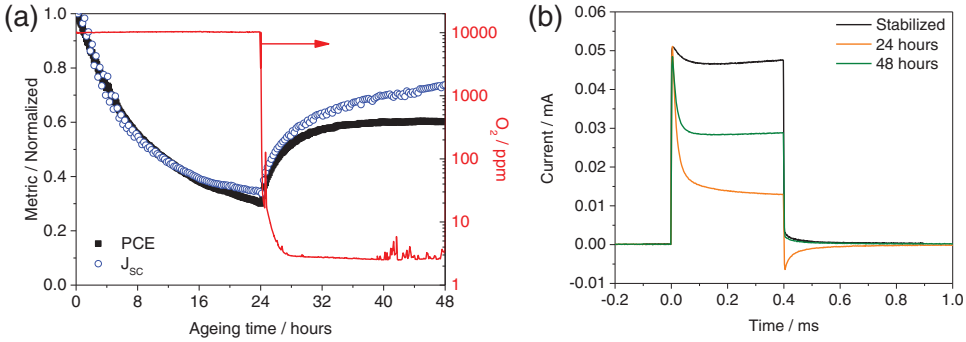

Figure 3. Aging data for a reference solar cell exposed to 1% O_2 during operation. After 24 h, the O_2 supply to the sample testing chamber is switched off. a) The relative solar cell PCE and J_{SC} is plotted against aging time (left axis), alongside the atmospheric concentration of O_2 (right axis). b) Transient photocurrent data before O_2 aging (stabilized), after 24 h and after 48 h.

"switches" the transient decay current from being negative (corresponding to charge injection) to positive (corresponding to charge extraction). Note the marginal changes in TPC current shortly after the LED switches on. Repeating this experiment on PSCs aged under 5% O_2 for 24 h did not observe a recovery in device performance during subsequent operation under N_2 (see the Supporting Information, Figure S6).

Further insight into the evolution of the solar cell during accelerated aging can be obtained through transient photovoltage measurements. From Figure 1b it was shown that during aging under 5% O_2, the solar cell V_{OC} underwent an approximately linear decrease over 24 h. **Figure 4** shows photovoltage decay kinetics, as measured through TPV, at distinct points in the experiment. It can be seen (Figure 4b) that the photovoltage decay time increases over the course of the experiment, from within the sub-microsecond resolution of our setup up to tens of microseconds. This trend has previously been observed in PBDTTT-EFT:$PC_{71}BM$ organic photovoltaic devices during burn-in, where in both cases the TPV measurements were performed under constant white light bias.[53] Because this does not necessarily allow for the internal conditions of the solar cell to be matched (e.g., due to differences in charge density) we also consider TPV kinetics under varying incident white light bias at distinct stages of the aging process. These specific results are presented in Figure 4c,d.

From Figure 4c it can be seen that upon adjusting the bias light intensity to set an open-circuit voltage of 0.71 V, the solar cell in its stabilized state exhibits a slower photovoltage decay compared against its aged state. Characteristic decay times – assuming monoexpontential kinetics – are 11 and 5 µs, respectively. We have repeated this experiment on an additional device from the same production batch and observed a similar trend when matching V_{OC} at 0.81 V (i.e., close to 1 sun conditions, see the Supporting Information, Figure S7). In Figure 4d, extracted photovoltage decay times are presented at different V_{OC} values at distinct stages in the aging experiment. Specifically, upon aging in 5% O_2 for 4 h, the relative loss in steady-state solar cell photocurrent is 50%. After 24 h, this loss now amounts to 90%, with the V_{OC} also being significantly reduced (see Figure 4b).

To interpret our TPV data, we first consider an appropriate mechanism which can be used to describe photovoltage decay in our solar cells. To the best of our knowledge, TPV data have not been published on $CH_3NH_3PbI_{3-X}Cl_X$ PSCs employing a mesoporous alumina scaffold, however several studies have considered photovoltage decay behavior in $CH_3NH_3PbI_3$ PSCs employing a mesoporous TiO_2 scaffold.[39,56,57] Critically, TPV decays in these device architectures were strongly biexponential, in contrast to the monoexponential behavior apparently observed here. O'Regan et al. proposed that under 1 sun conditions, photovoltage decays with a lifetime of around 1 µs correspond to the dominant electron/hole recombination channel.[39] The physical location of this recombination process was not confirmed, however related work suggested that the long-lifetime decay component relates to charge recombination within the TiO_2 scaffold[56,57] with the shorter component (up to several microseconds) quantifying carrier lifetime within the perovskite layer. Although we caution against the comparison of absolute TPV decay times between independent studies, due to likely variations in device preparation and measurement conditions, in our solar cells the volume fraction of TiO_2 is relatively low because the metal oxide exists as a compact cathode interface layer only. We therefore suggest that our TPV measurements are primarily sensitive to charge recombination within the perovskite layer. When V_{OC} is matched close to 1 sun conditions, the measured faster decays in devices aged for 4 h are likely a result of more recombination sites being present, a consequence of the increased number of electronic traps and mobile defects that account for the proposed loss in quasi-steady state photocurrent.[58–60] The extent to which mobile defects and electronics traps are linked is presently unknown, and whilst we acknowledge that our TPC/TPV measurements are primarily sensitive to processes that take place on the microsecond timescale, different kinetics could well be observed if these measurements are repeated on a timescale that is commensurate with defect mobility.[43–47]

To identify the underlying mechanisms behind the irreversible loss in PCE of the reference cells, we note that recent work on aged $CH_3NH_3PbI_3$ films identified a detrimental photochemical reaction involving oxygen.[61,62] Specifically, it was proposed that photogenerated electrons in the perovskite permit a reaction between the methylammonium organic cation and superoxide, a process that results in decomposition of $CH_3NH_3PbI_3$ with methylamine, PbI_2, I_2, and H_2O as byproducts:

$$CH_3NH_3PbI_3 + O_2^{\bullet -} \xrightarrow{\text{Deprotonation}} CH_3NH_2 + PbI_2 + 1/2\ I_2 + H_2O \quad (1)$$

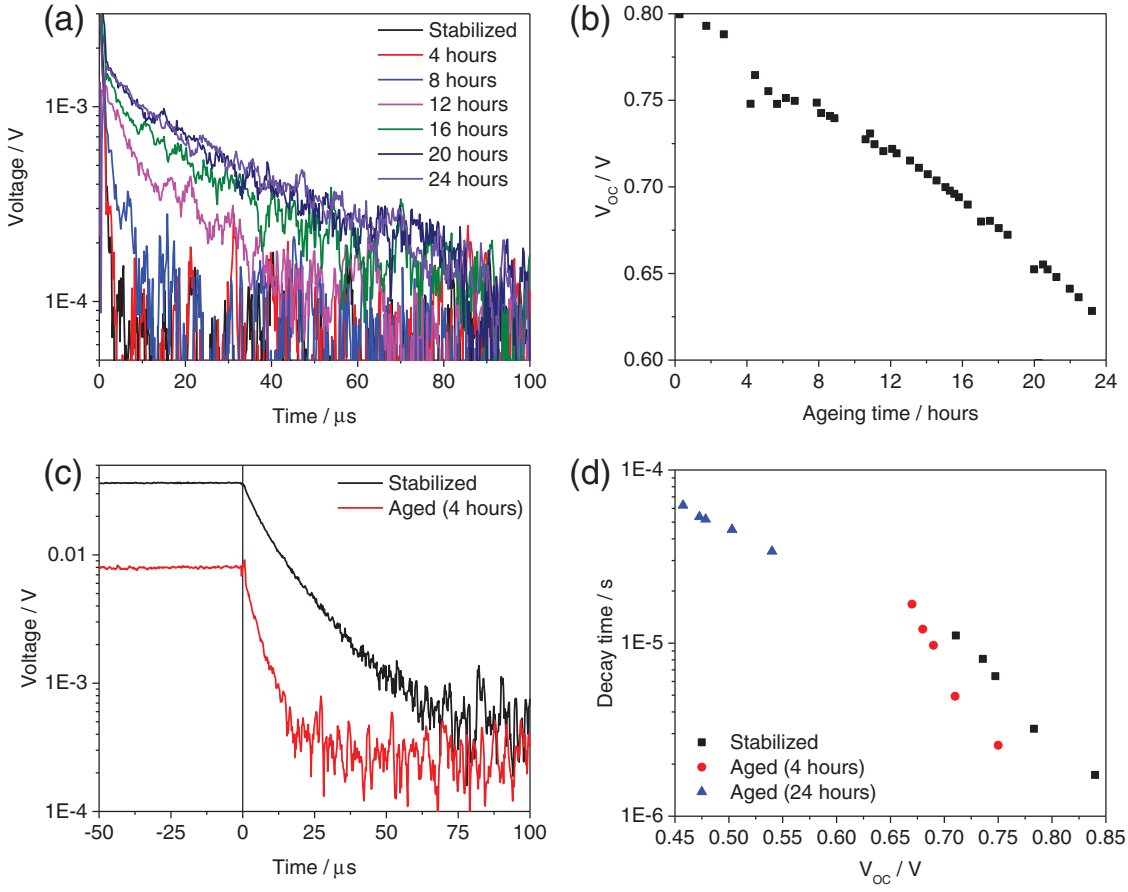

Figure 4. a) In situ transient photovoltage decay kinetics for a reference solar cell at different aging times under 5% O_2, as measured under constant white light bias (1 sun). For ease of comparison the decay profiles are presented after subtraction of V_{OC}. b) Absolute V_{OC} values of the solar cell during aging. c) Transient photovoltage decay kinetics for a nominally identical device aged under 5% O_2, with neutral density filters used to match device V_{OC} at 0.71 V. In this figure, 0 µs corresponds to the end of the LED perturbation pulse. The relative voltage perturbations for the device in its stabilized and aged state are 5% and 1%, respectively. d) Photovoltage decay times across a range of V_{OC} values for the same device in its stabilized and aged (5% O_2) states.

The damage caused to the perovskite layer by this process was shown to be linked to the efficiency of electron extraction; decomposition via photooxidation was slower when $CH_3NH_3PbI_3$ was interfaced to a mesoporous TiO_2 scaffold when compared against an equivalent perovskite film without an electron acceptor present,[62] indicating the importance of electron density in the perovskite when discussing the effects of photostability. We can understand this process on complete PSCs using $CH_3NH_3PbI_{3-X}Cl_X$ by undertaking the following straightforward experiment: two devices were stabilized and subsequently aged under 10% O_2 whilst being held at either short circuit or open circuit. The cell held at short circuit will have a relatively low average charge density since all photogenerated charges will be extracted rapidly. When the device is held at open-circuit, similar to an isolated film, the photogenerated charges cannot be extracted and so the charge density will be much higher. After aging, the devices were visually examined. As shown in **Figure 5**, we observe a striking difference in discoloration for devices held at the two conditions.

For the solar cell held continuously at open circuit, a significant discoloration is observed relative to the control (c.f. Figure 5a,c), with the underlying Au electrode more visible. Regions with a characteristic yellow hue are present across the substrate (photographs of the devices aged under 5% O_2 are presented in the Supporting Information, Figure S8). In contrast, the color changes between the control and the solar cell held at short

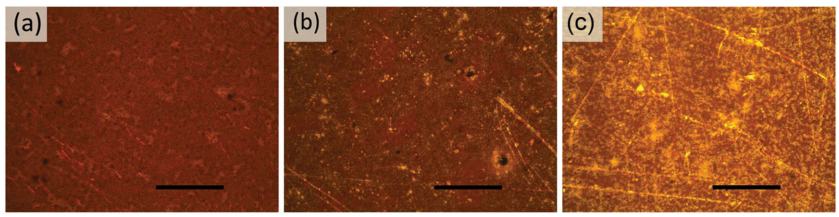

Figure 5. Optical microscopy images of reference solar cells aged for 24 h under 10% O_2. a) Control device which was not subject to aging, b) device held at short circuit throughout aging, and c) device held at open circuit throughout aging. Scale bar represents 0.5 mm.

circuit (Figure 5b) are less apparent. This straightforward test supports the literature discussed earlier and confirms that the oxygen tolerance of PSCs is strongly related to charge density within the perovskite layer. As a consequence, efforts to develop PSCs with enhanced O_2 stability should therefore aim to maintain a high efficiency of charge extraction, either through the use of conducting scaffolds or high performance compact electrode interface layers. However, clearly there is a conundrum here, since to obtain the maximum operating voltages and hence efficiency significant splitting of the quasi-Fermi levels for electrons and holes needs to be occurring during operation at maximum power point. Hence to reach the ultimate high efficiencies while maintaining high stability, it is likely that the intrinsic sensitivity of the perovskite to this reaction with oxygen will need to be reduced. This may be achieved via the reduction of residual defects in the perovskite layer that form during sample preparation,[63] or through chemical substitution (for example, by replacement of methylammonium with formamidinium or cesium).[64,65] Alongside these expected developments, we anticipate that related studies will also seek to clarify the role of non-perovskite phases in governing sample sensitivity. This would be particularly relevant when these phases are present by design, as can be the case with, for example, excess PbI_2.[66,67] In terms of module design, device stability will also be linked to the ability of oxygen to efficiently diffuse laterally and vertically through each layer in the solar cell. For example, for PSCs employing Spiro-MeOTAD, such as those investigated in this study, thin films of this material are known to form pinholes through which oxygen molecules may efficiently travel. Recent work has however demonstrated that the number of pinholes may be reduced by preparing the hole transport layer from a volatile solvent,[68] suggesting a straightforward strategy for mitigating this specific degradation pathway.

Lastly, to confirm that decomposition of the perovskite takes place within our reference solar cells, and relate these changes to our transient data, new PSCs were aged under 5% O_2 for 4 or 24 h. These devices were subsequently measured using XRD to provide information on the crystallinity and composition of the perovskite layer. Data are presented in **Figure 6**.

We attribute the relatively narrow peaks located at $2\theta = 14.08°$ and 28.35° to X-ray scattering from the (110) and (220) planes of the tetragonal perovskite phase.[2] The relatively low-intensity feature at $2\theta = 12.67°$ can be attributed to PbI_2,[3] its presence in the XRD pattern of the fresh device suggesting incomplete conversion of the perovskite precursor during device fabrication. For the aged samples, an 85% reduction in X-ray scattering intensity of the 110 perovskite reflection (at $2\theta = 14.08°$) is evidenced after 24 h relative to the fresh device. In contrast, the changes in X-ray scattering intensity after 4 h are minimal (approximately 1%), providing further support to our hypothesis that device degradation occurs over two distinct phases. Namely, phase (1) is the initial formation of mobile defects within the device, which reduce the efficiency of charge extraction in the cell and lead to a build-up of charge. Over time and under conditions of continued device illumination and oxygen exposure, these blocked charges will contribute toward the oxidation of the perovskite material, resulting in its decomposition (phase (2)).

In general, the XRD measurements of the aged devices show no clear correlation with either the level of amorphous content (that would likely modify the background level of X-ray scattering) or the amount of crystalline PbI_2, the latter inferred from the intensity of X-ray scatter at $2\theta = 12.6°$ (see Figure 6b). We suggest therefore that prolonged aging primarily induces the loss of mass content from the sample, with $CH_3NH_3PbI_{3-X}Cl_X$ breaking down – and the PSC undergoing irreversible degradation – due to the loss of methylamine and iodine from the sample during the second degradation phase.[61] In making this statement we acknowledge that the X-ray beam in these measurements samples an area of several mm^2 across the device, therefore providing an insight into average crystallinity only. To complement this dataset we also performed energy-dispersive X-ray spectroscopy (EDS) measurements on similarly aged devices to characterize their chemical composition (note that EDS was performed after removal of the Au electrode). The results of this experiment are summarized in **Figure 7**. Here, it can be seen that aging induces an increase in Pb content within the sample relative to the concentration of both C and I, with the largest increase taking place between 4 and 24 h aging. In addition, the absolute wt% of C and I decrease with aging (full EDS survey data are presented in the Supporting Information, Table S1), supporting our interpretation of the XRD data. When

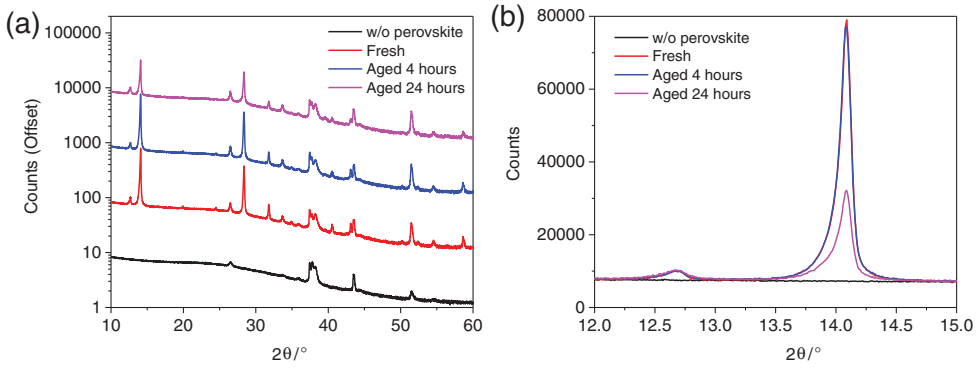

Figure 6. X-ray diffraction data for reference perovskite solar cells aged under 5% O_2. a) The XRD patterns have been offset for clarity. b) Raw data highlighting features over the 2θ range 12°–15° are presented. Note that data corresponding to "w/o perovskite" correspond to an equivalent solar cell structure without any perovskite material present (i.e., glass/FTO/TiO_2/Al_2O_3/Spiro-MeOTAD/Au).

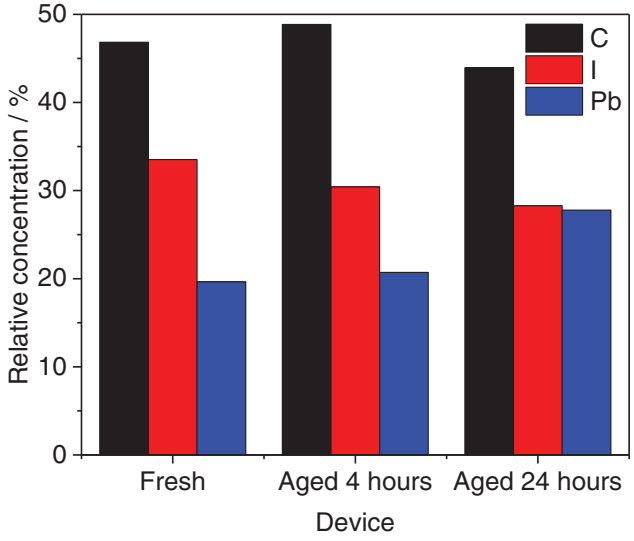

Figure 7. Composition analysis for perovskite solar cells aged under 5% O_2, as determined from EDS measurements. Here, the data have been normalized to consider the relative fractions of C, I, and Pb in each sample only.

combining these results with the data presented in Figures S6 and S8 (in the Supporting Information) we therefore conclude that prolonged PSC operation in the presence of oxygen results in the severe breakdown of the perovskite phase, with the spatially resolved level of degradation strongly influenced by the local ability to extract photogenerated charge carriers. Work is currently underway to measure the photovoltaic and composition characteristics of a PSC in situ to provide a quantifiable link between these properties.

3. Conclusions

Transient photocurrent and photovoltage measurements have been used to give insight into the behavior of model $CH_3NH_3PbI_{3-X}Cl_X$ perovskite solar cells operating in the presence of oxygen. Stress testing under these conditions evidences a reduction in solar cell efficiency that is dominated by a loss in photocurrent. This process occurs over two distinct phases: an initial semi-reversible screening of the built-in field of the solar cell that results from an increased defect density and, following extended O_2 exposure, breakdown of the light-harvesting perovskite layer itself. In addition to the relative concentration of oxygen present during testing (that is, the external conditions), the extent to which $CH_3NH_3PbI_{3-X}Cl_X$ undergoes photooxidation is strongly influenced by charge density and charge-extraction efficiency, in agreement with recent work on $CH_3NH_3PbI_3$ films. Our findings provide an important contribution toward understanding the operation of perovskite solar cells under working conditions, as well as identifying a rational framework toward mitigating oxygen degradation, helping to realize these devices as an efficient and stable PV technology.

4. Experimental Section

Materials and Solvents: Unless otherwise stated, all materials were purchased from Sigma-Aldrich or Alfa Aesar and used as received. Spiro-OMeTAD was purchased from Borun Chemicals.

Sample Preparation: For mesosuperstructured device fabrication, fluorine-doped tin oxide (FTO)-coated glass substrates (Pilkington, 7 Ω $\square^{-1}$) were first cleaned with detergent and deionized water, then with acetone and isopropanol, followed by oxygen plasma treatment. The electron-accepting TiO_2 compact layer was spin-coated (2000 rpm for 60 s) from a precursor solution prepared by adding titanium isopropoxide into a mixture of ethanol and diluted HCl. The relative amounts used were 70 µL titanium isopropoxide, 1 mL ethanol, and 7 µL 2 M HCl. After spin-coating, the sample was sintered at 500 °C. An alumina mesoporous scaffold was then deposited by spin-coating (2500 rpm for 60 s) a colloidal dispersion of 20 nm Al_2O_3 nanoparticles in isopropanol followed by drying at 150 °C. The perovskite layer was then spin-coated in air in a humidity-controlled chamber with 15–30% relative humidity (2000 rpm for 45 s) and annealed at 100 °C for 120 min. Spiro-OMeTAD hole-transport material was then deposited via spin-coating (2000 rpm for 45 s) a 0.0788 M solution in chlorobenzene, with additives of 0.0184 M lithium bis(trifluoromethanesulfonyl)imide (added in 0.61 M acetonitrile solution) and 0.0659M 4-tert-butylpyridine. Gold electrodes were deposited via thermal evaporation to complete the devices.

Sample Characterization–PCE: The current density–voltage (*J–V*) curves were measured (2400 Series SourceMeter, Keithley Instruments) under simulated AM 1.5 sunlight at 100 mW cm^{-2} irradiance generated by an Abet Class AAB Sun 2000 simulator, with the intensity calibrated with an NREL calibrated KG5 filtered Si reference cell. The mismatch factor was calculated to be less than 1%. The solar cells were masked with a metal aperture to define the active area of 0.0625 cm^{-2} and measured in a light-tight sample holder to minimize any edge effects and ensure that the reference cell and test cell are located during measurement in the same spot under the solar simulator. For the fast JV scans, cells were scanned from forward bias to short-circuit at a rate of 0.38 V s^{-1} after holding under illumination at 1.4 V for 5 s. The maximum power point was determined from these fast JV scans and the current was measured holding at this voltage for the stabilized power output measurements.

Sample Characterization–In situ IV, TPC, TPV: To minimize device degradation, solar cells were stored under vacuum or glovebox conditions before transfer to the aging setup. During each experiment the chamber was held at a slight overpressure, with the N_2 supply prefiltered (SGT Super Clean) to minimize residual oxygen, moisture and hydrocarbon content. Oxygen and water content was monitored in situ using a gas analyzer (Rapidox 3100D – Cambridge Sensotec) connected to the gas exit line of the sample chamber. A Newport Solar Simulator with equivalent AM 1.5 G 1-sun output was used to illuminate the entire device substrate; solar cell current–voltage characteristics were collected using a Keithley 2636 SMU. A 465 nm LED (LED465E, Thor Labs) was used as the light source for transient experiments, connected to an Agilent 33500B wavefunction generator and a purpose-built low-noise power supply. Solar cell transients were recorded by connecting the device to a Tektronix DPO 3032 oscilloscope. For TPC measurements, the device was connected to the 50 Ω input of the oscilloscope via a custom transimpedance amplifier. The 1 MΩ input of the oscilloscope was used for TPV measurements. White-light bias for TPV measurements was provided by the solar simulator. A custom-written LabView VI was used for instrument control and data acquisition (a looped sequence of IV, TPC, TPV measurements).

Sample Characterization–X-Ray Scattering: Coupled 2θ–θ scans of X-ray diffraction from perovskite devices were obtained using a Bruker D8 X-ray Diffractometer (step size 0.01°, scan time 40 min). Samples were measured under ambient conditions and low light to minimize sample degradation during measurement.

Sample Characterization–EDS: Measurements were performed using an FEI Philips XL30 sFEG with an EDS (EDAX) detector. An accelerating

voltage of 15 kV was used throughout, with EDS spectra acquired from a series of maps (50×50 μm^2) on each sample.

Supporting Information

Supporting Information is available from the Wiley Online Library or from the author.

Acknowledgements

This work was supported by SABIC and by the EPSRC, including by the Supergen Supersolar Consortium (EP/J017361/1) and the European Union Seventh Framework Program [FP7 2007-2003] under grant agreement 604032 of the MESO project. G.E.E. was supported by the EPSRC and Oxford Photovoltaics Ltd. through a Nanotechnology KTN CASE award. J.T.-W.W. acknowledges the Swire Educational Trust for supporting his D.Phil. study at Oxford. The authors thank Dr Sian Dutton (University of Cambridge) for access to XRD facilities and Dr Felix Deschler (University of Cambridge) for helpful discussions. The data underlying this publication are available at https://www.repository.cam.ac.uk/handle/1810/254858.

Received: January 4, 2016
Revised: March 24, 2016
Published online: April 26, 2016

[1] A. Kojima, K. Teshima, Y. Shirai, T. Miyasaka, *J. Am. Chem. Soc.* **2009**, *131*, 6050.
[2] M. M. Lee, J. Teuscher, T. Miyasaka, T. N. Murakami, H. J. Snaith, *Science* **2012**, *338*, 643.
[3] J. Burschka, N. Pellet, S. J. Moon, R. Humphry-Baker, P. Gao, M. K. Nazeeruddin, M. Gratzel, *Nature* **2013**, *499*, 316.
[4] M. A. Green, A. Ho-Baillie, H. J. Snaith, *Nat. Photonics* **2014**, *8*, 506.
[5] H. J. Snaith, *J. Phys. Chem. Lett.* **2013**, *4*, 3623.
[6] G. Hodes, *Science* **2013**, *342*, 317.
[7] J. H. Noh, S. H. Im, J. H. Heo, T. N. Mandal, S. I. Seok, *Nano Lett.* **2013**, *13*, 1764.
[8] G. E. Eperon, S. D. Stranks, C. Menelaou, M. B. Johnston, L. M. Herz, H. J. Snaith, *Energy Environ. Sci.* **2014**, *7*, 982.
[9] L. Protesescu, S. Yakunin, M. I. Bodnarchuk, F. Krieg, R. Caputo, C. H. Hendon, R. X. Yang, A. Walsh, M. V. Kovalenko, *Nano Lett.* **2015**, *15*, 3692.
[10] C. C. Stoumpos, C. D. Malliakas, M. G. Kanatzidis, *Inorg. Chem.* **2013**, *52*, 9019.
[11] F. Deschler, M. Price, S. Pathak, L. E. Klintberg, D. D. Jarausch, R. Higler, S. Huttner, T. Leijtens, S. D. Stranks, H. J. Snaith, M. Atature, R. T. Phillips, R. H. Friend, *J. Phys. Chem. Lett.* **2014**, *5*, 1421.
[12] Z. K. Tan, R. S. Moghaddam, M. L. Lai, P. Docampo, R. Higler, F. Deschler, M. Price, A. Sadhanala, L. M. Pazos, D. Credgington, F. Hanusch, T. Bein, H. J. Snaith, R. H. Friend, *Nat. Nanotechnol.* **2014**, *9*, 687.
[13] S. D. Stranks, H. J. Snaith, *Nat. Nanotechnol.* **2015**, *10*, 391.
[14] J. S. Luo, J. H. Im, M. T. Mayer, M. Schreier, M. K. Nazeeruddin, N. G. Park, S. D. Tilley, H. J. Fan, M. Gratzel, *Science* **2014**, *345*, 1593.
[15] L. T. Dou, Y. Yang, J. B. You, Z. R. Hong, W. H. Chang, G. Li, Y. Yang, *Nat. Commun.* **2014**, *5*, 5404.
[16] S. Yakunin, M. Sytnyk, D. Kriegner, S. Shrestha, M. Richter, G. J. Matt, H. Azimi, C. J. Brabec, J. Stangl, M. V. Kovalenko, W. Heiss, *Nat. Photonics* **2015**, *9*, 444.
[17] G. D. Niu, X. D. Guo, L. D. Wang, *J. Mater. Chem. A* **2015**, *3*, 8970.
[18] T. Leijtens, G. E. Eperon, N. K. Noel, S. Habisreutinger, P. Petrozza, H. J. Snaith, *Adv. Energy. Mater.* **2015**, *5*, 1500963.
[19] K. Leo, *Nat. Nanotechnol.* **2015**, *10*, 574.
[20] A. Y. Mei, X. Li, L. F. Liu, Z. L. Ku, T. F. Liu, Y. G. Rong, M. Xu, M. Hu, J. Z. Chen, Y. Yang, M. Gratzel, H. W. Han, *Science* **2014**, *345*, 295.
[21] X. Li, M. Tschumi, H. W. Han, S. S. Babkair, R. A. Alzubaydi, A. A. Ansari, S. S. Habib, M. K. Nazeeruddin, S. M. Zakeeruddin, M. Gratzel, *Energy Technol.* **2015**, *3*, 551.
[22] W. S. Yang, J. H. Noh, N. J. Jeon, Y. C. Kim, S. Ryu, J. Seo, S. I. Seok, *Science* **2015**, *348*, 1234.
[23] T. Baikie, Y. N. Fang, J. M. Kadro, M. Schreyer, F. X. Wei, S. G. Mhaisalkar, M. Graetzel, T. J. White, *J. Mater. Chem. A* **2013**, *1*, 5628.
[24] J. L. Yang, B. D. Siempelkamp, D. Y. Liu, T. L. Kelly, *ACS Nano* **2015**, *9*, 1955.
[25] J. A. Christians, P. A. M. Herrera, P. V. Kamat, *J. Am. Chem. Soc.* **2015**, *137*, 1530.
[26] A. M. A. Leguy, Y. Hu, M. Campoy-Quiles, M. I. Alonso, O. J. Weber, P. Azarhoosh, M. van Schilfgaarde, M. T. Weller, T. Bein, J. Nelson, P. Docampo, P. R. F. Barnes, *Chem. Mater.* **2015**, *27*, 3397.
[27] S. N. Habisreutinger, T. Leijtens, G. E. Eperon, S. D. Stranks, R. J. Nicholas, H. J. Snaith, *Nano Lett.* **2014**, *14*, 5561.
[28] J. W. Liu, S. Pathak, T. Stergiopoulos, T. Leijtens, K. Wojciechowski, S. Schumann, N. Kausch-Busies, H. J. Snaith, *J. Phys. Chem. Lett.* **2015**, *6*, 1666.
[29] G. D. Niu, W. Z. Li, F. Q. Meng, L. D. Wang, H. P. Dong, Y. Qiu, *J. Mater. Chem. A* **2014**, *2*, 705.
[30] H. P. Zhou, Q. Chen, G. Li, S. Luo, T. B. Song, H. S. Duan, Z. R. Hong, J. B. You, Y. S. Liu, Y. Yang, *Science* **2014**, *345*, 542.
[31] G. E. Eperon, S. N. Habisreutinger, T. Leijtens, B. J. Bruijnaers, J. J. van Franeker, D. W. de Quilettes, S. Pathak, R. J. Sutton, G. Grancini, D. S. Ginger, R. A. Janssen, A. Petrozza, H. J. Snaith, *ACS Nano* **2015**, *9*, 9380.
[32] J. M. Frost, K. T. Butler, F. Brivio, C. H. Hendon, M. van Schilfgaarde, A. Walsh, *Nano Lett.* **2014**, *14*, 2584.
[33] I. C. Smith, E. T. Hoke, D. Solis-Ibarra, M. D. McGehee, H. I. Karunadasa, *Angew. Chem. Int. Ed.* **2014**, *53*, 11232.
[34] J. Liu, Y. Z. Wu, C. J. Qin, X. D. Yang, T. Yasuda, A. Islam, K. Zhang, W. Q. Peng, W. Chen, L. Y. Han, *Energy Environ. Sci.* **2014**, *7*, 2963.
[35] H. S. Kim, C. R. Lee, J. H. Im, K. B. Lee, T. Moehl, A. Marchioro, S. J. Moon, R. Humphry-Baker, J. H. Yum, J. E. Moser, M. Gratzel, N. G. Park, *Sci. Rep.* **2012**, *2*, 591.
[36] J. M. Ball, M. M. Lee, A. Hey, H. J. Snaith, *Energy Environ. Sci.* **2013**, *6*, 1739.
[37] T. Leijtens, E. T. Hoke, G. Grancini, D. J. Slotcavage, G. E. Eperon, J. M. Ball, M. De Bastiani, A. R. Bowring, N. Martino, K. Wojciechowski, M. D. McGehee, H. J. Snaith, A. Petrozza, *Adv. Energy. Mater.* **2015**, *5*, 1500962.
[38] H. J. Snaith, A. Abate, J. M. Ball, G. E. Eperon, T. Leijtens, N. K. Noel, S. D. Stranks, J. T. W. Wang, K. Wojciechowski, W. Zhang, *J. Phys. Chem. Lett.* **2014**, *5*, 1511.
[39] B. C. O'Regan, P. R. F. Barnes, X. E. Li, C. Law, E. Paomares, J. M. Marin-Beloqui, *J. Am. Chem. Soc.* **2015**, *137*, 5087.
[40] R. S. Sanchez, V. Gonzalez-Pedro, J. W. Lee, N. G. Park, Y. S. Kang, I. Mora-Sero, J. Bisquert, *J. Phys. Chem. Lett.* **2014**, *5*, 2357.
[41] W. Tress, N. Marinova, T. Moehl, S. M. Zakeeruddin, M. K. Nazeeruddin, M. Gratzel, *Energy Environ. Sci.* **2015**, *8*, 995.
[42] J. M. Frost, K. T. Butler, A. Walsh, *APL Mater.* **2014**, *2*, 081506.
[43] C. Eames, J. M. Frost, P. R. F. Barnes, B. C. O'Regan, A. Walsh, M. S. Islam, *Nat. Commun.* **2015**, *6*. 7497.
[44] Y. Zhang, M. Z. Liu, G. E. Eperon, T. C. Leijtens, D. McMeekin, M. Saliba, W. Zhang, M. de Bastiani, A. Petrozza, L. M. Herz, M. B. Johnston, H. Lin, H. J. Snaith, *Mater. Horiz.* **2015**, *2*, 315.

[45] Y. Zhao, C. J. Liang, H. M. Zhang, D. Li, D. Tian, G. B. Li, X. P. Jing, W. G. Zhang, W. K. Xiao, Q. Liu, F. J. Zhang, Z. Q. He, *Energy Environ. Sci.* **2015**, *8*, 1256.
[46] Z. G. Xiao, Y. B. Yuan, Y. C. Shao, Q. Wang, Q. F. Dong, C. Bi, P. Sharma, A. Gruverman, J. S. Huang, *Nat. Mater.* **2015**, *14*, 193.
[47] S. van Reenen, M. Kemerink, H. J. Snaith, *J. Phys. Chem. Lett.* **2015**, *6*, 3808.
[48] H. S. Kim, N. G. Park, *J. Phys. Chem. Lett.* **2014**, *5*, 2927.
[49] L. K. Ono, S. R. Raga, S. H. Wang, Y. Kato, Y. B. Qi, *J. Mater. Chem. A* **2015**, *3*, 9074.
[50] D. Bryant, S. Wheeler, B. C. O'Regan, T. Watson, P. R. F. Barnes, D. Worsley, J. Durrant, *J. Phys. Chem. Lett.* **2015**, *6*, 3190.
[51] N. K. Noel, A. Abate, S. D. Stranks, E. S. Parrott, V. M. Burlakov, A. Goriely, H. J. Snaith, *ACS Nano* **2014**, *8*, 9815.
[52] Z. Li, F. Gao, N. C. Greenham, C. R. McNeill, *Adv. Funct. Mater.* **2011**, *21*, 1419.
[53] I. Hwang, C. R. McNeill, N. C. Greenham, *J. Appl. Phys.* **2009**, *106*, 094506.
[54] A. J. Pearson, P. E. Hopkinson, E. Couderc, K. Domanski, M. Abdi-Jalebia, N. C. Greenham, *Org. Electron.* **2016**, *30*, 225.
[55] A. Baumann, S. Väth, P. Rieder, M. C. Heiber, K. Tvingsted, V. Dyakonov, *J. Phys. Chem. Lett.* **2015**, *6*, 2350.
[56] J. W. Lee, T. Y. Lee, P. J. Yoo, M. Gratzel, S. Mhaisalkar, N. G. Park, *J. Mater. Chem. A* **2014**, *2*, 9251.
[57] V. Roiati, S. Colella, G. Lerario, L. De Marco, A. Rizzo, A. Listorti, G. Gigli, *Energy Environ. Sci.* **2014**, *7*, 1889.
[58] J. H. Im, H. S. Kim, N. G. Park, *APL Mater.* **2014**, *2*. 081510.
[59] Z. G. Xiao, Q. F. Dong, C. Bi, Y. C. Shao, Y. B. Yuan, J. S. Huang, *Adv. Mater.* **2014**, *26*, 6503.
[60] J. Xu, A. Buin, A. H. Ip, W. Li, O. Voznyy, R. Comin, M. Yuan, S. Jeon, Z. Ning, J. J. McDowell, P. Kanjanaboos, J. P. Sun, X. Lan, L. N. Quan, D. H. Kim, I. G. Hill, P. Maksymovych, E. H. Sargent, *Nat. Commun.* **2015**, *6*, 7081.
[61] N. Aristidou, I. Sanchez-Molina, T. Chotchuangchutchaval, M. Brown, L. Martinez, T. Rath, S. A. Haque, *Angew. Chem. Int. Ed.* **2015**, *54*, 8208.
[62] F. T. F. O'Mahony, Y. H. Lee, C. Jellett, S. Dmitrov, D. T. J. Bryant, J. R. Durrant, B. C. O'Regan, M. Graetzel, M. K. Nazeeruddin, S. A. Haque, *J. Mater. Chem. A* **2015**, *3*, 7219.
[63] W. Zhang, M. Saliba, D. T. Moore, S. K. Pathak, M. T. Hörantner, T. Stergiopoulos, S. D. Stranks, G. E. Eperon, J. A. Alexander-Webber, A. Abate, A. Sadhanala, S. Yao, Y. Chen, R. H. Friend, L. A. Estroff, U. Wiesner, H. J. Snaith, *Nat. Commun.* **2015**, *6*, 6142.
[64] G. E. Eperon, S. D. Stranks, C. Menelaou, M. B. Johnston, L. M. Herz, H. J. Snaith, *Energy Environ. Sci.* **2014**, *7*, 982.
[65] J. Lee, D. Kim, H. Kim, S. Seo, S. M. Cho, N. Park, *Adv. Energy Mater.* **2015**, *5*, 1501310.
[66] F. Liu, Q. Dong, M. K. Wong, A. B. Djurišić, A. Ng, Z. Ren, Q. Shen, C. Surya, W. K. Chan, J. Wang, A. M. C. Ng, C. Liao, H. Li, K. Shih, C. Wei, H. Su, J. Dai, *Adv. Energy. Mater.* **2016**, *6*, 1502206.
[67] D. Bi, W. Tress, M. I. Dar, P. Gao, J. Luo, C. Renevier, K. Schenk, A. Abate, F. Giordano, J. C. Baena, J. Decoppet, S. M. Zakeeruddin, M. K. Nazeeruddin, M. Grätzel, A. Hagfeldt, *Sci. Adv.* **2016**, *2*, 1501170.
[68] L. K. Ono, S. R. Raga, M. Remeika, A. J. Winchester, A. Gabea, Y. Qi, *J. Mater. Chem. A* **2015**, *3*, 15451.